Published on-line on November 26, 2012, in

APPLIED PHYSICS LETTERS **101**, 224102 (2012)

http://dx.doi.org/10.1063/1.4768925

http://link.aip.org/link/doi/10.1063/1.4768925

Plasma flares in high power impulse magnetron sputtering

Pavel A. Ni, Christian Hornschuch,[a] Matjaž Panjan, and André Anders[b]

Lawrence Berkeley National Laboratory, 1 Cyclotron Road, Berkeley, California 94720, USA

a) on leave from the University of the German Armed Forces, Neubiberg, Germany
b) Corresponding Author.
Dr. Andre Anders
Lawrence Berkeley National Laboratory
1 Cyclotron Road, MS 53
Berkeley, CA 94720, USA
Tel. +1-510-486-6745
Fax +1-510-486-4374
aanders@lbl.gov

ACKNOWLEDGEMENTS

We gratefully acknowledge the use of fast cameras offered by LBNL's Heavy Ion Fusion Sciences Program. We thank Rueben Mendelsberg and Joe Wallig for help. C.H. was support by the German Armed Forces, M.P. by a grant of the Fulbright Foundation, and A.A. acknowledges support by the Assistant Secretary for Energy Efficiency and Renewable Energy, Office of Building Technology of the U.S. Department of Energy. This work was supported by the U.S. Department of Energy under Contract No. DE-AC02-05CH11231.

Abstract

Self-organized ionization zones and associated plasma flares were recorded with fast cameras in side-on view. Flare velocities were estimated to be about 20,000 m/s suggesting that the local tangential field E_ξ is about 2000 V/m based on a concept where flare-causing electrons are initially ejected by $\mathbf{E}_\xi \times \mathbf{B}$ drift. At distances of 10 mm and greater from the target, where the electric field is very small, plasma flares are guided by the magnetic field **B**.

High power impulse magnetron sputtering[1-3] (HiPIMS) is an emerging technology in the field of ionized physical vapor deposition.[4] When a sputtering magnetron discharge is pulsed to very high power, typically two orders of magnitude above the average power, the target provides secondary electrons and an intense flux of neutrals composed of sputtered atoms and gas atoms.[5] The secondary electrons are subject to complicated motion in non-uniform electric and magnetic fields cleverly designed to trap electrons in a closed drift.[6,7] Drifting energetic electrons are very likely to cause ionizing collisions with neutral atoms. The high degree of ionization of sputtered atoms allows for self-ion-assisted deposition of thin films.

The peak current in HiPIMS can reach hundreds of amperes for small magnetrons, and several kiloamperes for large, industrial magnetrons. Current transport across magnetic field lines is known to be governed by instabilities as opposed to classical diffusion.[8] HiPIMS discharges are not an exception: the high electric current suggests that waves and instabilities play a critical role.[9,10] This understanding is supported by recent observations of plasma structures traveling along the target's racetrack. The structures were called inhomogeneities, regions of enhanced luminosity, and plasma bunches,[11] bright regions and rotating structures,[12] spokes,[13] or ionization zones.[14,15] We will stick with the term ionization zone in the remainder of this contribution. Fast framing and streak camera images showed that ionization zones travel in the same direction as the electron's $\mathbf{E} \times \mathbf{B}$ drift but with only about 10% of the electron drift velocity[11,12,14] (**E** and **B** are the local electric and magnetic field, respectively).

The theoretical description of such structures is still in its infancy. It was proposed that the structures are intimately related to the fluxes of electrons and atoms from the target,[15] as opposed to fluxes from the background. The ionization rate depends on both the density of energetic electrons and atoms to be ionized[16]

$$\left(\frac{\partial n_i}{\partial t}\right)_{ionization} = K_\alpha n_a n_e \qquad (1)$$

where $K_\alpha = \int f_e(v)\, v\, \sigma_{ea}(v)\, dv$ is the ionization rate coefficient, containing the electron velocity distribution function $f_e(v)$ and the ionization cross section $\sigma_{ea}(v)$. It was further proposed[15] that the motion of ionization zones along the racetrack is associated with "evacuation" of ions from the pre-target region to the target by the electric field of the presheath. Ion evacuation

exposes neutrals behind the densest plasma to drifting energetic electrons, where "behind" refers to the frame of reference of drifting electrons. By ion generation and evacuation, the region of strongest ionization is shifted in the $\mathbf{E}\times\mathbf{B}$ direction, which appears as motion of plasma. According to the ionization and evacuation model, the region of most intense excitation and ionization moves but not the plasma. In this sense, the observed motion relates to a phase velocity, not a group velocity.

Other approaches to the phenomenon have been proposed. Most recently a connection was made to Alfvén's critical ionization velocity,[13]

$$v_{Alfven} = \left(\frac{2eU_{ion}}{m_n} \right)^{1/2} . \qquad (2)$$

where U_{ion} is the ionization potential and m_n the mass of the neutral atoms to be ionized. A strong increase in the ionization rate should be expected when the relative velocities of ions and neutrals across the magnetic field exceed v_{Alfven}. Experimentally observed velocities of ionization zones[11,12,14] are indeed greater than the critical velocity; which is, for the case of niobium,[14] $v_{Alfven}\left(\mathrm{Nb}\right) = 3750$ m/s.

In this contribution, we focus on getting experimental data and interpreting them in the framework of the ionization zone model.[15] According to this model, the edge of a dense plasma region does not only have an electric field in the *z*-direction (normal to the target) but in the ξ-direction (along the racetrack, parallel to the target surface). In the case of a disk target with a circular racetrack, the ξ-direction can be readily expressed by the azimuthal angle,[11-13] e.g. labeled φ in ref.[11,17], or θ in ref.[14] The coordinate ξ is more general since the racetrack can have a non-circular shape, as in the case of rectangular or "linear" targets.[1] As a consequence of the tangential field $\mathbf{E}_\xi$ (or azimuthal field $\mathbf{E}_\theta$ for a target with a circular racetrack), the closed drift of electrons is disrupted. Instead of drifting over the target's racetrack, the electrons get deflected in the $\mathbf{E}_\xi\times\mathbf{B}$ direction when they encounter a dense plasma zone. This deflection manifests itself as a "jet" or "plasma flare" leaving the target. Here we investigate such plasma flares with greater time and space resolution than before, and we focus on side-on views using a streak camera and a fast frame camera. This allows us to gain more information on size and development of plasma flares with the goal to provide guidance for the development of theoretical models of HiPIMS operation.

An unbalanced magnetron (US Inc., now MeiVac Inc.) with a 76 mm (3 inch) diameter, 6.25 mm (1/4 inch) thick niobium target was operated in argon background gas. The cylindrical anode was mounted flush with the target, which allowed us to have an unobstructed side view of the region next to the target, including the target's surface plane.

The power was supplied by a commercial HiPIMS power supply (model SIPP by Melec, maximum 1 kV, 1 kA). Pulse duration, repetition frequency, peak current, argon gas pressure etc. were similar to our previous work[14] and we will specify values with each result given here.

Streak images were taken with a Hamamatsu C7700 streak camera. Detector amplification was always kept low to stay well below the non-linear region leading to saturation. The image dimensions were 1344 pixels in space and 1024 pixels for the time axis. The light intensity was recorded with 14 bit resolution. Fast frame images were taken with a Princeton Instruments PIMAX 1024 camera equipped with a microchannel plate amplifier. The exposure time and the dynamic intensity resolution were 10 ns and 16 bit, respectively. The intensities are presented in false color using the color scale "royal" of the image processing software *ImageJ*.[18]

The magnetron and its pre-target region were viewed side-on through a quartz window, which was protected by a shutter. The shutter was opened only when recording an image. The streak camera's slit, opened to 10 pixels width, was aligned with the axis of symmetry of the magnetron (*z*-direction). As explained in our previous work,[14] a 1.5 mm diameter alumina ceramic rod was placed on axis, aligned with the camera slit, in order to block the view behind the rod. Thereby, only emission from plasma in front of the rod was recorded, hence avoiding the interpretation issues that we would have looking across front and back racetrack regions. While the original streak images have a horizontal *z*-axis, all images were rotated 90° in counterclockwise direction for a more conventional presentation that has the time-axis going horizontally from left to right. To be consistent, frame images were rotated, too, showing the *z*-axis in the same way as the streak images.

Using different streak sweep speeds gives immediate insight into the degree of pattern formation by self-organization. In Fig. 1, bright ionization zones travel into and out of the field of view of the slit every few microseconds. The spacings of the zones are sometimes regular but more often the "rhythm" of bright zones seems to be affected by several factors, resulting in what appears to be almost unpredictable brightness pattern.

In the following we select individual streak and frame images to elucidate the mechanism of the formation and properties of plasma flares. The propagation of plasma from the near-target region is best seen with a high sweep speed (short sweep time). Fig. 2 shows an example taken with 2 μs sweep time relatively early in a 80 μs HiPIMS pulse. Only the velocity component in *z*-direction, $v_{flare} = \Delta z/\Delta t$, can be evaluated since the streak camera's slit is aligned along the *z*-direction. Figure 2 indicates (i) the greatest light intensity is very close to the target, extending just a few millimeters; (ii) the initial propagation velocity from the target is about 2×10^4 m/s, with a tendency to slow as the distance from the target increases; (iii) as the flare propagates, the recorded light intensity increases to reach a maximum at a distance of about 8 mm.

While Fig. 2 shows a typical flare, not all flares appear this way. Fig. 3 shows a streak image obtained with a sweep time of 5 μs. Same flares, like the one close to the right of Fig. 3, seems to start some millimeters away from the target, not close to the target as usual. In other examples, like the one in the center of Fig. 3, there is practically no tilt, which will be discussed later. In the supplementary material (here given on the last page), at a compilation of 100 streak images is provided, each taken with a sweep duration of 20 μs at the end of 80 μs, 500 A peak current pulses. All images show that flares start very close to the target. Using the Child-Langmuir approximation we find a sheath thickness less than 0.5 mm, which cannot be resolved in our images.

Frame images, such as Figs. 4 and 5, show that ionization zones over the target are not symmetric, and that plasma flares are often tilted in space. When increasing the voltage of the multichannel plate image amplifier one can see plasma emission in greater distances from the target. Flares appear structured and sometimes look like jets (Fig. 5). The shapes of plasma flares near the sides of the target, as well as far from the target, suggest that the plasma is guided along the magnetic field lines rather than showing cross-field drift. This can be expected when the electric field is small ($\mathbf{E}\times\mathbf{B}$ vanishes) and the magnetron is unbalanced (magnetic field lines leave the target region).

Flares show a great variety of appearances, often non-periodic spacings, and ongoing modulation and evolution. This suggest that a description of periodic azimuthal wave structures, e.g. of the generalized drift wave type,[12] is perhaps not applicable, or at least greatly distorted by nonlinear feedbacks. Most images support the proposition[15] that the *edge* of a dense ionization zone, i.e. the location of the greatest density gradient, is a region having an electric field in ξ-direction because most flares originate there (e.g., the central flare in Fig. 3). An electric field $\mathbf{E}_\xi$ causes drift of electrons in the $\mathbf{E}_\xi\times\mathbf{B}$ direction, where they cause excitation and ionization. We see is the optical emission "fingerprint" of inelastic collisions of electrons with atoms and ions. In this work, the measured intensity is not spectrally resolved. However, there are plenty of data in the literature on HiPIMS plasma composition obtained by particle spectrometry and optical emission spectroscopy.[1-4] Those data indicate a high percentage of ions, especially in the later phase of each HiPIMS pulse.[3] When interpreting optical emission intensities we have to consider the spectral response function of the measuring instrument. It is primarily determined by the spectral sensitivity function of the detector and also affected by the spectral transmittance of the vacuum chamber window, lenses, and other optical components. In this work, the cameras are sensitive in the visible spectral range, which implies that much of the emission from ions cannot be seen since the most intense spectral lines are in the ultraviolet (UV) spectral region. Therefore, absence of light, or low intensity, has to be evaluated with caution since UV light is very likely to be present but not detected. This is one of the possible interpretations of the unusual start of the flare on the right side of Fig. 3.

One also needs to consider the shape of the energy-dependent cross sections of excitation and ionization. Generally, cross sections have thresholds (excitation and ionization energies, respectively) and maxima that are species-dependent. The maximum for ionization is typically in the region below 100 eV for atoms, and at higher energies for singly and multiply charged ions.[19] Since secondary electrons can pick up kinetic energy corresponding to up to the full applied voltage, here 630-680 V, their energy is on the high-energy side relative to the cross section's maximum. As energetic electrons lose energy by interacting with other electrons, atoms, and ions, the likelihood for excitation and ionization actually *increases* until the electron's energy is on the low energy side of the maximum. This dependency may lead to greater optical emission intensity in the region where the secondary electrons have lost some energy, and where the density of electrons is enhanced by ionization processes. Therefore one should expect the emission intensity to reach a maximum as the flare propagates from the target, as observed in Fig. 2.

Assuming that flares are associated with an $\mathbf{E}_\xi\times\mathbf{B}$ electron drift, the observed slight slowdown implies that the electric field $E_\xi(z)$ drops faster than the magnetic field $B(z)$, since

$v_z = E_\xi / B$. The magnetic field was carefully mapped[20] and gave about 100 mT in 1 mm and 50 mT in 10 mm above the racetrack. One can deduce that E_ξ must be about 2000 V/m and 75 V/m in 1 mm and 10 mm distance, respectively. The vector $\mathbf{E}_\xi$ points in the direction of travel of the ionization zone, otherwise the flare would not travel *away* from the target. One should expect that $\mathbf{E}_\xi$ also causes ion acceleration tangential to the racetrack, which has been observed,[17,21] and for which we will present detailed, energy-resolved data in a separate contribution.

Flare velocities showed a correlation with current (or power, or plasma density – all of them are related): at the beginning of a HiPIMS pulse they have greater tilt (smaller velocity) in streak images than later in the pulse (*cf*. Figs. 1(b) - (d)). This is consistent with the concept that the field $\mathbf{E}_\xi$ is associated with the density gradient.[15] Sometimes one can find a slow flare between fast flares. Therefore, a simple current-flare velocity relation does not exist. Rather, the evolution of a flare depends not only on the general discharge but on the local plasma conditions.

The occasional lack of tilt and even slight left tilt of a flare in a streak image (Fig. 3) can be explained by considering that the flares can be titled in space. They usually trail the ionization zones, which travel over the racetrack in the $\mathbf{E}\times\mathbf{B}$ direction with a speed of 7000 ± 2000 m/s for the case of niobium target (Table I of ref.[14]). Images suggest that the flares are affected by the local conditions. A flare may not always be trailing the ionization zone but occasionally shoot under an angle ahead of it. As the flare velocity is generally 2-4 times faster than the ionization zone velocity, a flare could appear in the streak camera's slit at some distance from the target *before* the ionization zone enters the field of view. Hence the impression of a "negative velocity" can appear.

In summary, fast frame camera studies confirmed that ionization zones traveling over the target's racetrack emit plasma flares, which appear to be caused by electrons leaving the closed drift region. At high sweep speed of the streak camera, the flares are tilted in $z-t$ images, and the flare velocity in *z*-direction was determined to be typically 2×10^4 m/s. This velocity was generally lower at the beginning of the pulse when the current was still low and the plasma was not yet as dense as later in the pulse. Ionization zones and associated plasma flares exhibit patterns typical for non-equilibrium, self-organized systems. However, the patterns evolve throughout a pulse and the positions and sizes of plasma flares cannot be precisely predicted. The transverse electric field $\mathbf{E}_\xi$ at a zone edge was estimated to be about 2000 V/m in a millimeter-region above the target, and much weaker for $z > 10$ mm.

References

[1] A. Ehiasarian, in *Plasma Surface Engineering Research and its Practical Applications*, edited by R. Wei (Research Signpost, Kerala, India, 2008), p. 35.

[2] K. Sarakinos, J. Alami, and S. Konstantinidis, Surf. Coat. Technol. **204,** 1661 (2010).

[3] J. T. Gudmundsson, N. Brenning, D. Lundin, and U. Helmersson, J. Vac. Sci. Technol. A **30,** 030801 (2012).

[4] U. Helmersson, M. Lattemann, J. Bohlmark, A. P. Ehiasarian, and J. T. Gudmundsson, Thin Solid Films **513,** 1 (2006).

[5] A. Anders, J. Čapek, M. Hála, and L. Martinu, J. Phys D: Appl. Phys. **45,** 012003 (2012).

[6] J. W. Bradley, S. Thompson, and Y. A. Gonzalvo, Plasma Sources Sci. Technol. **10,** 490 (2001).

[7] A. Rauch and A. Anders, Vacuum **89,** 53 (2012).

[8] E. Choueiri, Phys. Plasmas **8,** 1411 (2001).

[9] D. Lundin, U. Helmersson, S. Kirkpatrick, S. Rohde, and N. Brenning, Plasma Sources Sci. Technol. **17,** 025007 (2008).

[10] N. Brenning, R. L. Merlino, D. Lundin, M. A. Raadu, and U. Helmersson, Phys. Rev. Lett. **103,** 225003 (2009).

[11] A. Kozyrev, N. Sochugov, K. Oskomov, A. Zakharov, and A. Odivanova, Plasma Physics Reports **37,** 621 (2011).

[12] A. P. Ehiasarian, A. Hecimovic, T. de los Arcos, R. New, V. Schulz-von der Gathen, M. Böke, and J. Winter, Appl. Phys. Lett. **100,** 114101 (2012).

[13] N. Brenning and D. Lundin, Phys. Plasmas **19,** 093505 (2012).

[14] A. Anders, P. Ni, and A. Rauch, J. Appl. Phys. **111,** 053304 (2012).

[15] A. Anders, Appl. Phys. Lett. **100,** 224104 (2012).

[16] V. E. Golant, A. P. Zhilinsky, I. E. Sakharov, and S. C. Brown, *Fundamentals of Plasma Physics* (Wiley, New York, 1980).

[17] D. Lundin, P. Larsson, E. Wallin, M. Lattemann, N. Brenning, and U. Helmersson, Plasma Sources Sci. Technol. **17,** 035021 (2008).

[18] W. Rasband, *ImageJ 1.44p, downloaded from* http://imagej.nih.gov/ij (National Institute of Health, 2011).

[19] H. Tawara and T. Kato, Atomic Data and Nuclear Data Tables **36,** 167 (1987).

[20] A. Rauch, R. Mendelsberg, J. M. Sanders, and A. Anders, J. Appl. Phys. **111,** 083302 (2012).

[21] P. Poolcharuansin, B. Liebig, and J. W. Bradley, Plasma Sources Sci. Technol. **21,** 015001 (2012).

Figure Captions

FIG. 1. Streak images of HiPIMS discharges (Ar 0.7 Pa, 50 pulses per second, 630-680 V, 500 A peak) using different pulse HiPIMS lengths and sweep durations: (a) 300 μs pulse, 200 μs sweep, (b) 180 μs pulse, 100 μs sweep, (c) 80 μs pulse, 50 μs sweep, (d) 80 μs pulse, 20 μs sweep, (e) 80 μs pulse, 10 μs sweep, and (f) 80 μs pulse, 5 μs sweep.

FIG. 2 High resolution streak image (sweep duration 2 μs) of a plasma flare recorded in about the middle of a 80 μs HiPIMS pulse (Ar 0.6 Pa, 50 pulses per second, 670 V, 500 A peak current).

FIG. 3 Streak image of plasma flares recorded in the second half of a 80 μs HiPIMS pulse (Ar 0.7 Pa, 50 pulses per second, 630 V, 500 A peak current). For compilation of such images see http://dx.doi.org/10.1063/1.4768925.1

FIG. 4 Frame image with an exposure time of 10 ns, showing two ionization zones and flares (the long shadow in the center is the rod used for streak imaging).

FIG. 5 As figure 4 but with greater image amplification. The shape of plasma near the edges of the target indicates that plasma follows the magnetic field line structure when the electric field is weak. The shadow in the top left is caused by the window's shutter.

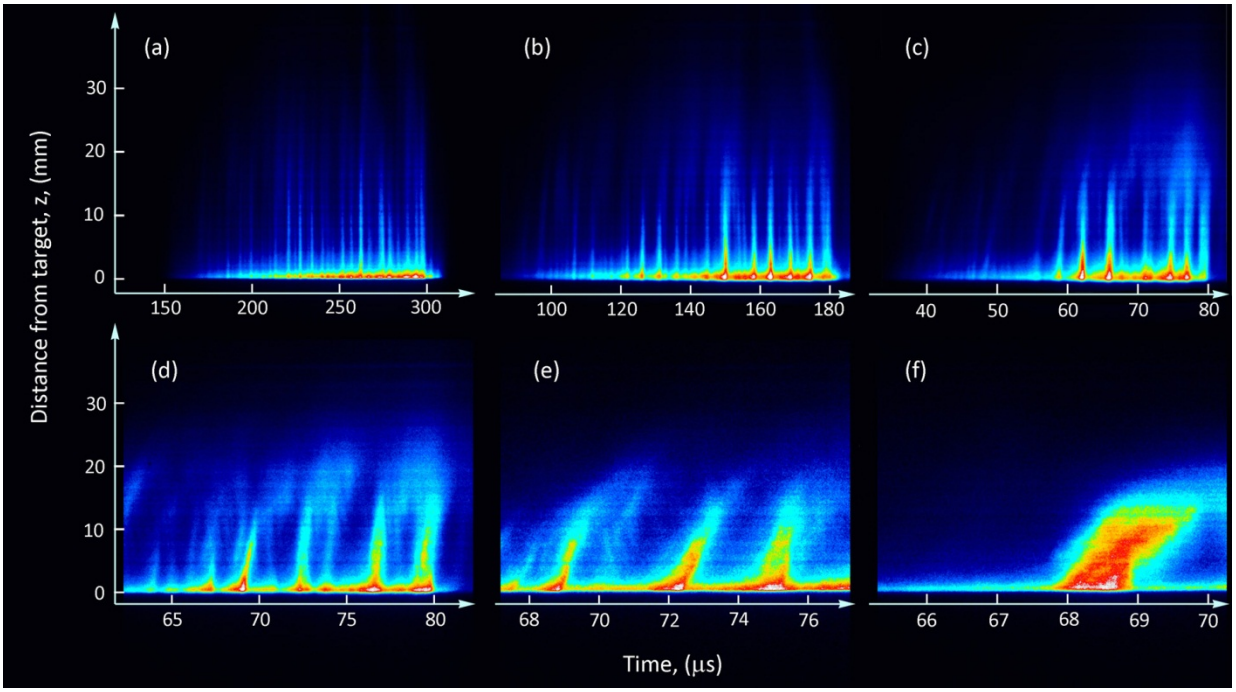
(a)
(b)
(c)
(d)
(e)
(f)
Distance from target, z, (mm)
Time, (μs)
0
10
20
30
150
200
250
300
100
120
140
160
180
40
50
60
70
80
65
70
75
80
68
70
72
74
76
66
67
68
69
70

FIG. 1

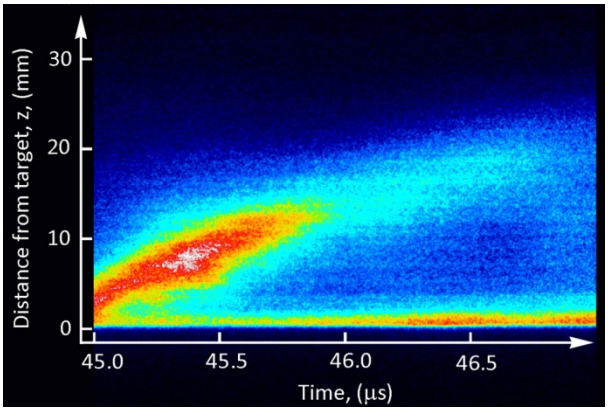

FIG. 2

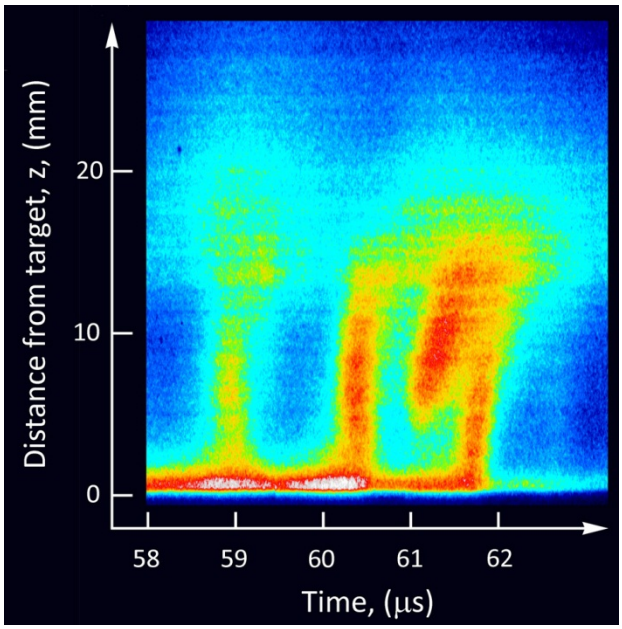

FIG. 3

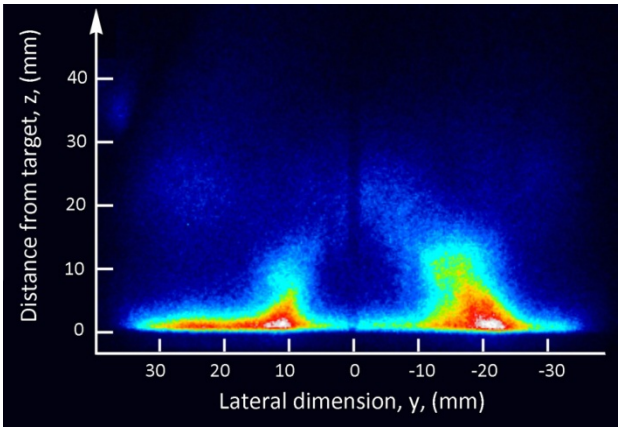
Distance from target, z, (mm)
40
30
20
10
0
30
20
10
0
-10
-20
-30
Lateral dimension, y, (mm)

FIG. 4

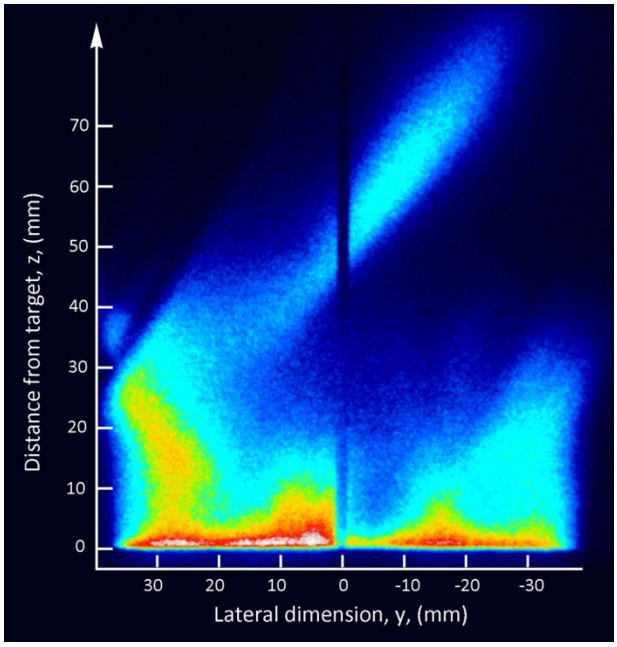
Distance from target, z, (mm)
70
60
50
40
30
20
10
0
30
20
10
0
-10
-20
-30
Lateral dimension, y, (mm)

FIG. 5

Supplemental material: Animated GIF file showing 100 streak images (each from a different pulse).

http://dx.doi.org/10.1063/1.4768925.1